In Situ Structural Variations of Individual Particles of an Al_2O_3-Supported Cu/Fe Spinel Oxygen Carrier During High-Temperature Oxidation and Reduction

W. H. Harrison Nealley, Anna Nakano, Jinichiro Nakano and James P. Bennett

Abstract Physical and chemical degradation of the oxygen-carrier materials during high-temperature redox exposures may affect the overall efficiency of the chemical looping process. Therefore, studying real-time physical and chemical changes in these materials when exposed to repeated redox cycles is essential for further development of chemical looping technology. In this work, the National Energy Technology Laboratory's Al_2O_3-supported Cu/Fe spinel oxygen carrier, in the form of a $CuO \cdot Fe_2O_3$ solid solution, was examined in situ during 3-h exposures to either oxidizing or reducing environments at 800 °C using a controlled atmosphere heating chamber in conjunction with a confocal scanning laser microscope. A compilation of the physical changes of individual particles using a controlled atmosphere confocal microscope and the microstructural/chemical changes documented using a scanning electron microscope will be discussed.

Keywords Chemical looping · Fossil energy · Oxygen carrier

Introduction and Background

The emission of CO_2 due to carbon-based industrial processes is one of the main contributors to the amount of greenhouse gases in the atmosphere [1]. Measures have been taken to reduce the emissions from sites that produce CO_2 such as power plants,

W. H. H. Nealley (✉) · A. Nakano · J. Nakano · J. P. Bennett
U.S. Department of Energy National Energy Technology Laboratory,
1450 Queen Ave, Albany, OR 97321, USA
e-mail: william.nealley@netl.doe.gov

W. H. H. Nealley
Oak Ridge Institute for Science and Education, 100 ORAU Way, Oak Ridge,
TN 37380, USA

A. Nakano · J. Nakano
AECOM, P.O. Box 618, South Park, PA 15129, USA

J. Nakano et al. (eds.), *Advanced Real Time Imaging II*, The Minerals,
Metals & Materials Series, https://doi.org/10.1007/978-3-030-06143-2_3

smelters, and gasifiers. Part of the core mechanism of CO_2 emissions lies with the oxidation of carbon in fossil fuels.

If air is used to provide the necessary O_2 to support the combustion process, the presence of N_2, which plays a minimal role in the combustion process relative to O_2, reduces the overall energy efficiency because it must be heated to the process temperature. This also makes subsequent carbon capture of the exhaust more difficult [2].

The carbon capturing would be more efficient if the oxidizer used for combustion produces pure CO_2 exhaust without any other gas species present. Chemical looping combustion can produce pure CO_2 by utilizing oxygen-carrier materials. These materials act by exchanging oxygen during oxidation/reduction (redox) cycles. This technique would be more feasible if using solid oxygen carriers versus those in a liquid or gaseous state pose a number of financial and technical problems [3].

A viable material for this purpose must be resistant to physical and chemical attritions over long periods of time involving high temperatures and a varying gas environment. Multiple metal oxides, both single-metallic and bimetallic, have been tested for their use in this application [4, 5]. Cu and Fe oxides were found to be two of the best candidates due to their ability to oxidize and reduce repeatedly [6]. However, the metal oxide carriers are usually supported on a ceramic, such as Al_2O_3, with which the oxygen carriers of Cu and Fe oxides have been shown to react at chemical looping combustion temperatures [7, 8]. Further improvements in Cu- and Fe-based oxygen carriers would support the material development.

At the National Energy Technology Laboratory (NETL), a Cu–Fe spinel-based material supported on Al_2O_3 is being developed as an oxygen-carrier (OC) candidate for chemical looping applications [9]. The present work continues a study with this material. A previous study discussed part of the material characteristics in high-temperature environments while undergoing repeated redox cycles [3].

Materials and Methods

Material

The OC studied in this work was developed by NETL and manufactured by Nexceris using solid-state mixing. The sample composition was analyzed using X-ray fluorescence spectroscopy (XRF and Rigaku ZSX Primus II) and determined to be 37.49 wt%CuO, 31.32 wt%Fe_2O_3, and 31.19 wt%Al_2O_3. The X-ray diffraction analysis (XRD and Rigaku Ultima IV XRD spectrometer) of as-received OC sample confirmed the presence of two crystalline phases: spinel and alumina. Details of this material can be found in Siriwardane et al. [10].

Confocal Microscopy

For in situ analysis, the samples were placed inside a halogen-lamp furnace (Yonekura) with a quartz observation window, which was attached to a confocal scanning laser microscope (CSLM and Olympus OLS 3100) (Fig. 1). The furnace was also equipped with a gas delivery system.

In situ observations were conducted by first heating a sample to 800 °C at 800 °C/min in synthetic air (79 vol%N_2–21 vol%O_2). Once heating was completed, the air (oxidizing gas) flow was either maintained or switched to a reducing gas mixture of 10 vol%CO–90 vol%Ar (10CO–90Ar hereafter). This was followed by a 5-min hold to stabilize temperature. After the hold, the material's surface was scanned with a 408 nm laser and with white light once every 5 min for the first 30 min of each gas exposure and every 30 min thereafter. 3D data obtained from the scans were used to analyze individual particles' volume change during gas exposures. The gas flow rate was 50 mL/min throughout the test. No particle stirring was performed; that is, sample evaluations were conducted in a static environment other than a gas flowing through the chamber.

The samples were subjected to up to four 180-min gas exposures with cooling to ambient temperature between each exposure (Fig. 2). Due to the extended length of the test, in some cases, samples were cooled to room temperature and stored overnight in the chamber in the synthetic air with no flow before the next gas exposure. Gas exposures were designed to simulate extended redox cycles and followed the progression: oxidation (Ox), oxidation–reduction (Ox–Red), oxidation–reduction–oxidation (Ox–Red–Ox), and oxidation–reduction–oxidation–reduction (Ox–Red–Ox–Red). Following the final gas exposure of each test, the sample was quenched with a

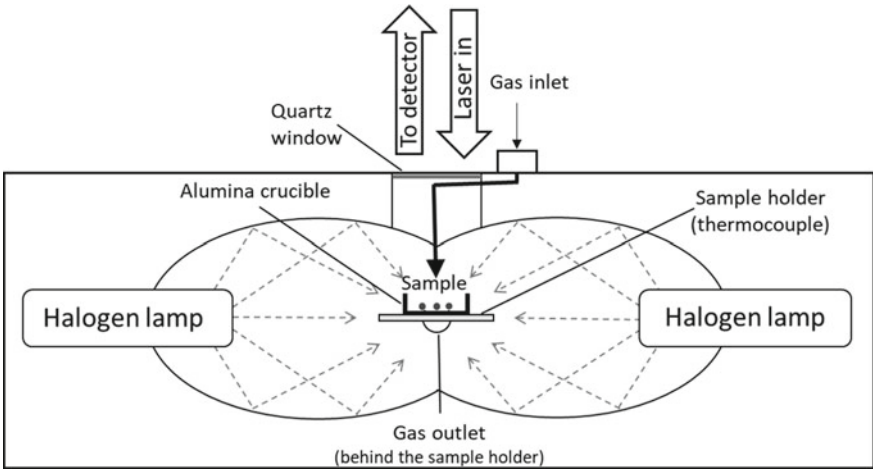

Fig. 1 A schematic of the CSLM heating chamber; reproduced with permission from Nealley et al. [3]

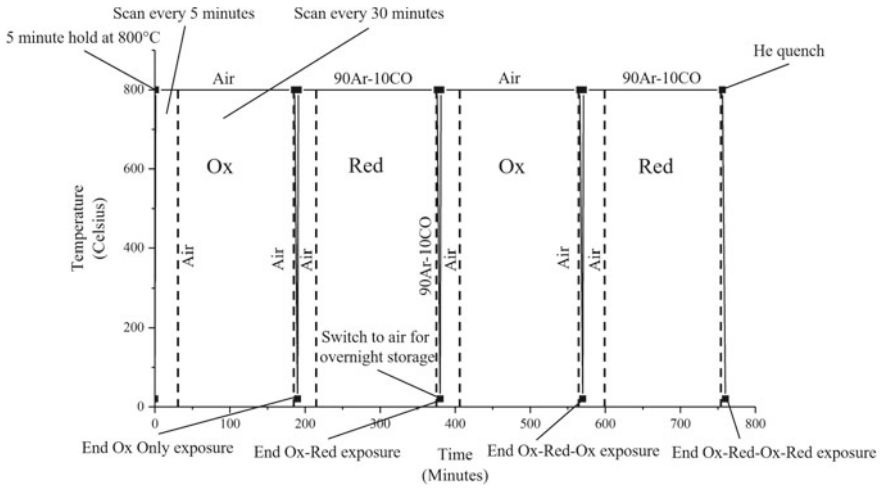

Fig. 2 Example of the experimental temperature profile for the extended gas exposure tests. "Ox"-oxidizing gas; "Red"-reducing gas

60 mL/min flow of He. The samples were then removed from the CSLM chamber and stored in plastic bags inside a desiccator at ambient temperature for post-exposure analysis.

A special procedure for the volume change analysis was developed using Olympus' microanalytical software (LEXT). The uncertainty in the volume measurement was determined to be approximately 1.99%. Since the crucible bottom was not perfectly flat, the volume was measured twice to account for the minor variations. This uncertainty is specific to each data point and reported as error bars (Fig. 3).

Electron Microscopy

Cross-sections of the samples were analyzed by a scanning electron microscope (SEM and FEI Inspect F) with energy-dispersive X-ray spectroscopy (EDX and Oxford INCA Wave).

Results and Discussion

In Situ Observations

Data from laser and white-light scans were used to generate three-dimensional representations of the particles and analyze volume change. For all the tests, during

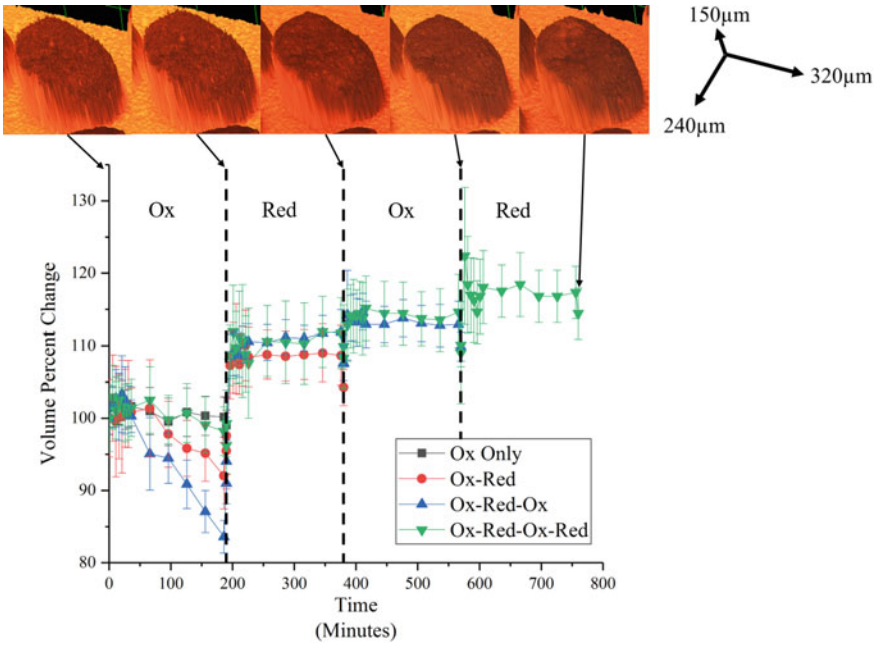

Fig. 3 Volume change measured during exposures relative to the respective particles' initial volumes (100%); the dashed lines indicate the end of one gas exposure and the beginning of another; in situ CSLM images from the Ox–Red–Ox–Red exposure are shown with their corresponding times at 800 °C

the initial oxidation (Ox), the sample tended to decrease in overall volume (Fig. 3). Assuming the original spinel structure was stable under the test conditions during oxidation, volume change was likely caused by sintering at 800 °C. It has been reported Cu/Fe spinel exhibits strong sintering-resistance under similar conditions of air oxidation, 50 vol%H_2 reduction, and 850 °C exposure temperature [11]. Note that the material used in those experiments was prepared via sol–gel combustion synthesis, whereas the present samples were prepared by mechanical mixing [10]. It is possible that the structural differences created by those manufacturing methods would influence the sintering behavior. Furthermore, the material in Wang et al. had already been sintered at 950 °C during the sample preparation procedure [11]. It is not certain whether the sample used for this study was appreciably sintered during the manufacturing process. Note, no sample heating prior to the experimental exposures was performed in this work.

During the following reducing gas exposure (Red), a rapid and substantial jump in volume was noted, indicating that the sample was rapidly altered immediately after exposure to the 10CO–90Ar gas. For the next Ox and Red gas exposures, sample exhibited the step-like volume change with a sharp increase at the beginning of each exposure.

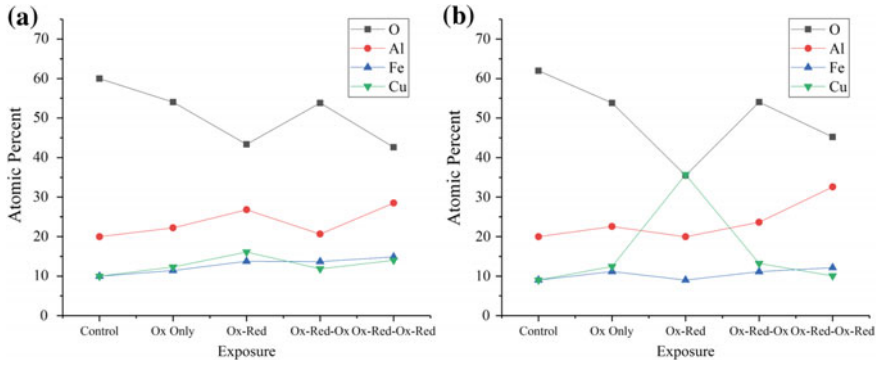

Fig. 4 Average elemental compositions of inner spinel grains plotted over exposure conditions; averages were produced from the five-EDX points taken near the center of the spinel grain; randomly selected spinel grains were measured near the center (**a**) and at the edge (**b**) of the bulk particle

Microstructural Changes

Control Sample (Before Exposure)

A control sample taken from the as-received batch and subjected to no gas exposure showed uniform elemental distribution within inner grains with roughly equal concentrations of Fe and Cu, based on EDX analysis. The location of a grain within the bulk particle did not affect these results.

Sample Quenched After the First Oxidation

The composition of the sample exposed to air for three hours showed negligible microstructural variations from the control sample in the spinel grains (Figs. 4a,5a). No significant differences were observed between the center grain and the edge grain (Fig. 4a, b).

Sample Quenched After the Ox–Red Cycle

The sample that had been exposed to air followed by 10CO–90Ar showed ubiquitous microstructural alterations within inner grains (grain aggregates) making up the carrier particle. The spinel grains broke down to at least two separate phases upon reduction (Fig. 5b). EDX analysis indicated a correlation between the dark regions and Fe concentration as well as the light, needle-like regions and Cu concentration. Additionally, it was observed that Fe-rich micron particles were beginning to appear around the edges of the bulk particle during the reduction exposure. It is not certain if these particles are a new phase that formed or the original matrix depleted in

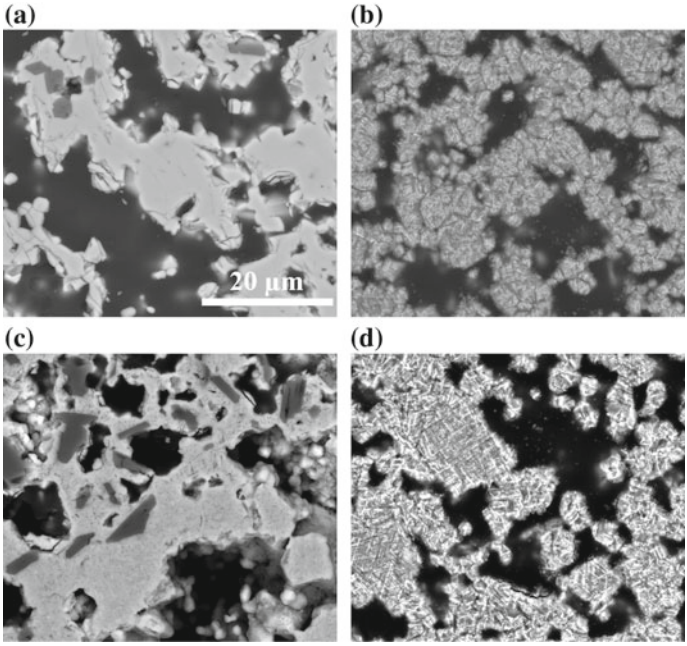

Fig. 5 Successive SEM images at 5000× of center spinel grains after Ox (**a**), Ox–Red (**b**), Ox–Red–Ox (**c**), and Ox–Red–Ox–Red (**d**)

Cu (or enriched with Fe). It was reported that at 800 °C in a reducing atmosphere of pure CH_4, the $CuO \cdot Fe_2O_3$ solid solution transformed into magnetite (Fe_3O_4), wüstite (FeO), delafossite ($CuFeO_2$), cuprous oxide (Cu_2O), and metallic Cu via lattice oxygen transfer and direct decomposition [11]. These phases may have existed in the present samples, which would explain the presence of the Fe-rich and Cu-rich regions. Further analysis using transmission electron microscopy is underway to confirm. Finally, grain boundaries on the order of a few hundred nanometers in width started to be visible at this stage.

Sample Quenched After the Ox–Red–Ox Cycle

The elemental distribution within the spinel phase after the Ox–Red–Ox gas exposure was found to be more uniform than in the quenched sample from the Ox–Red cycle. The Fe-rich particles on the surface of the bulk particle were still present. This is corroborated by the findings in Wang et al. that showed differentiation between the Fe-rich and Cu-rich phases after reoxidation [12]. A gradient in the oxygen partial pressure across the particle/grain aggregate may affect phase stability. Nanometer-scale voids formed within the matrix grains (Fig. 5c).

Sample Quenched After the Ox–Red–Ox–Red Cycle

This exposure series' results are somewhat similar to the Ox–Red sample. The phase separation within the grains was apparent (Fig. 5d). However, unlike in the O–Red exposure, the Cu-rich phase tended to form closer to the grain edges.

The Fe-rich formations on the surface observed after the Ox–Red cycle were also present in this sample. This time, they were found across the bulk particle, but not ubiquitous. Additionally, some of them were observed to be accompanied by an adjacent, but distinct, Cu-rich formation.

Conclusions

NETL's Cu/Fe spinel was investigated at 800 °C in both oxidizing and reducing atmospheres using a CSLM equipped with a furnace. Volume changes in individual particles were measured in situ to characterize how the material is altered by this high-temperature exposure. Particle volumes were noted to decrease during initial oxidation and then found to increase slightly during the subsequent reduction and oxidation exposures. SEM analysis showed that samples were relatively unchanged during initial oxidation but exhibited significant microstructural changes after the subsequent reduction, showing a separation of Cu- and Fe-rich regions, each with distinct morphology. The material also returned to a more uniform elemental distribution if oxidized a second time. However, the phase separation that was observed could result in changes in the oxygen carrier's performance over longer periods of time; future work is planned to investigate this question.

Acknowledgements This work was performed in support of the US Department of Energy's Fossil Energy Advanced Combustion Program. The research was executed through NETL Research and Innovation Center's Advanced Combustion effort. Research performed by AECOM Staff was conducted under the RES contract DE-FE-0004000. The authors wish to thank Mr. Matt Fortner for metallography.

Figure 1 reprinted with permission from Nealley et al.: Springer, JOM, Structural changes and material transport in Al_2O_3-supported Cu/Fe spinel particles in a simulated chemical looping combustion environment, Nealley WHH, Nakano A, Nakano J, Bennett JP, Copyright (2018).

The authors declare that they have no competing financial interest.

References

1. Metz B, Davidson OR, Bosch PR, Dave RL, Meyer A (eds) (2007) Mitigation. Contribution of working group III to the fourth assessment report of the intergovernmental panel on climate change, IPCC, 2007. Cambridge University Press, Cambridge
2. Hossain MM, de Lasa HI (2008) Chemical-looping combustions (CLC) for inherent CO_2 separations—a review. Chem Eng Sci 63:4433–4451
3. Nealley WHH, Nakano A, Nakano J, Bennett JP (2018) Structural changes and material transport in Al_2O_3-supported $CuFe_2O_4$ particles in a simulated chemical looping combustion environment. JOM 70(7):1232–1238
4. Lyngfelt A (2011) Oxygen carriers for chemical looping combustion—4000 h of operational experience. Oil Gas Sci Tech 66:161–172
5. Wang X, Chen Z, Hu M, Tian Y, Jin X, Ma S, Xu T, Hu Z, Liu S, Guo D, Xiao B (2017) Chemical looping combustion of biomass using metal ferrites as oxygen carriers. Chem Eng J 312:252–262
6. Voitic G, Hacker V (2016) Recent advancements in chemical looping water splitting for the production of hydrogen. RSC Adv 6:9867–9896
7. Hu W, Donat F, Scott SA, Dennis JS (2016) The interaction between CuO and Al_2O_3 and the reactivity of copper aluminates below 1000 °C and their implication on the use of the Cu–Al–O system for oxygen storage and production. RSC Adv 6:113016–113024
8. Liu W, Ismail M, Dunstan MT, Hu W, Zhang Z, Fennell PS, Scott SA, Dennis JS (2015) Inhibiting the interaction between FeO and Al_2O_3 during chemical looping production of hydrogen. RSC Adv 5:1759–1771
9. Bayham S, Straub D, Weber J (2017) Operation of the NETL chemical looping reactor with natural gas and a novel Copper-Iron material. NETL-PUB-20912; NETL technical report series; U.S. Department of Energy, National Energy Technology Laboratory, Morgantown, WV
10. Siriwardane R, Riley J, Bayham S, Straub D, Tian H, Weber J, Richards G (2018) 50-kWth methane/air chemical looping combustions tests with commercially prepared CuO–Fe_2O_3-alumina oxygen carrier with two different techniques. App Energy 213:92–99
11. Wang B, Yan R, Zhao H, Zheng Y, Liu Z, Zheng C (2011) Investigation of chemical looping combustion of coal with $CuFe_2O_4$ oxygen carrier. Energy Fuels 25:3344–3354
12. Wang B, Ma Q, Wang W, Zhang C, Mei D, Zhao H, Zheng C (2017) Effect of reaction temperature on the chemical looping combustions of coal with $CuFe_2O_4$ combined oxygen carrier. Energy Fuels 31:5233–5245